Boiling Heat Transfer Control by Micro-/Nano-Texturing of Metallic Heat-Spreading Devices

WCMNM 2021

Tatsuhiko Aizawa[1], Naoki Ono[2]

[1] *Surface Engineering Design Laboratory, SIT, Japan*
[2] *Shibaura Institute of Technology, Japan*

Abstract

High waste of heats generated from high-power transistors, LIDAR (Laser Imaging Detection and Ranging) and high power lasers must be efficiently transferred to cooling media with much higher heat flux than the normal criticality on the metallic surface. Among several approaches, the micro-/nano-textured aluminum and copper devices were fabricated to enhance the boiling heat transfer process to the subcooled water. The pure aluminum device with concave microtextures was first built by the plasma printing to describe the boiling heat transfer behavior with comparison to the bare aluminum plate. Next, the pure copper device with convex microtextures was developed by the wet plating to discuss the effect of microtextures on the heat transfer characteristics under the forced water cooling.

Keywords: Boiling heat transfer, Micro-/nano-texturing, Aluminium, Copper, Critical heat flux (CHF), Superheat, Micro-bubbles, Reynolds number

1. Introduction

Since the first notice on the problem of achieving compact, high-performance forced cooling in VLSI (Very-Large Scale Integrated) circuits [1], how to improve the capacity to cool down the energy-consuming devices and systems has grown up as the most essential issue of heat and mass transfer engineering. Micro-fluid channel heatsink in single phase was the first idea to improve the heat transfer between the heated surface and the cooling media. As surveyed in [2-4], numerical calculations were performed to optimize the micro-channel network. The enhancement of boiling heat transfer became the second approach [5].

In general, there are several heat transfer processes even by heat convection mechanism; e.g., the natural flow convection, the forced flow convection and the boiling heat transfer. Among them, this boiling heat transfer process provides the highest heat flux condition in practice [6]. However, the heat and mass transfer mechanism with phase transformation becomes more complex to be controlled for enhancement of this boiling heat transfer process. In the literature, new ideas were proposed to enhance this process. In addition to the micro-porous surface design in [5], the micro-structured surface design by spray cooling [7], micro-/nano-scale surface modification [8, 9], and wettability-controlled surface design [10] were developed to improve the boiling hear transfer process beyond the critical heat flux (CHF) limit [6]. As partially surveyed in [11], the nanoscale morphology of heat-dissipating media became important to enhance the heat transfer on the heating surface even with phase transformation.

After introduced by [6], three items to govern this boiling heat transfer are taken into account to describe the heat transfer with phase transformation and to consider how to control this process. First, nonlinear relationship between the heat flux and the superheating temperature is considered as illustrated in Figure 1. The logarithmic heat flux (ln (q)) takes off at B from the linear relation between ln (q) and ln (ΔT), which is observed in A – B for the natural convection flow heat transfer. Phase transformation from the liquid to its gaseous phase, or, the local boiling, commences at this point of B. The liquid water locally transforms to the vapor. The isolated vapors grow by themselves, gradually agglomerate among them on the heating surface and take off from the surface by buoyancy in B to D through C. In this regime, the heat flux significantly increases with increasing the superheat because of the latent heat by boiling, the mass transfer from liquid water to vapor, and the local convection flow. Approaching to the point of D, those growing vapors coalesce with each other to form a vapor film. Once this film locally forms on the heating surface, the heat transfer deteriorates by this film thermal conductance. At the point of D, the whole surface is covered by this vapor film; the heat flux becomes maximum at this point. Since D is physically unstable, further increase of heat flux induces the snap-through from the point of D to its neighboring stable point of F. If the constituent material for heating plate had sufficiently high melting temperature enough not to be melt down during this snap-through, the heat transfer process advances in stable from F to G in Figure 1. However, most of heating plates melt down or burn out after this snap-through behavior. On the way back by decreasing ΔT, this heat transfer process accompanies with another nonlinearity.

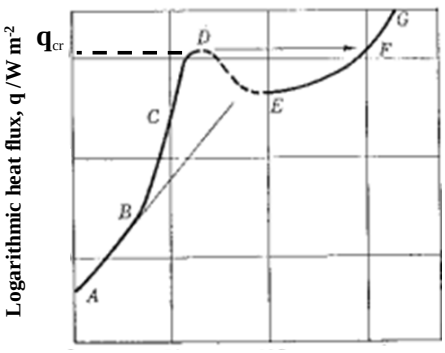

Figure 1. The relationship of the heat flux to the superheating temperature [6].

Every heat exchanging system and device has been

designed after this relationship. The feasible heat flux is limited by the critical heat flux in practice. To be free from this engineering constraint, this relationship must be modified by non-traditional heat transfer process.

In second, the phase transformation in the liquid water and vapor system stands on the nucleation of vapor bubbles on the heating surface. Most of theories on the nonlinear mechanics for heat transfer [6] and buckling mechanics [12] presume the geometric imperfections on the heating surface and on the shell structure, respectively. Figure 2 illustrates a nucleation stage of bubble formed at the wedge on the heating surface. For simplicity, the initial bubble shape is modeled by a sphere with its radius of r_c; then, the superheating temperature is inversely proportional to this r_c. Hence, the bubble size is controlled as small as possible to locally increase ΔT and to commence the boiling heat transfer in the early stage of ln (q) – ln (ΔT) relationship in Figure 1. In practice, there are very few studies to decrease the wedge depth, to increase the wedge density on the heating surface, to regularize the distribution of wedges and to control this regularity in the wedge alignment.

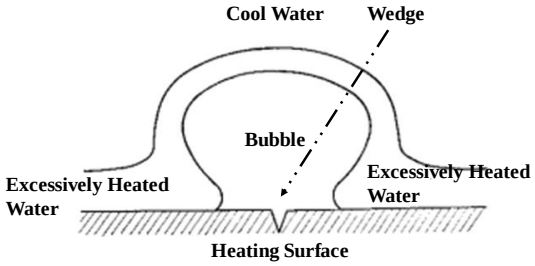

Figure 2. Traditional bubble nucleation model for phase transformation from liquid water to vapor bubble at the wedge on the heating surface [6].

In third, each growing bubble after nucleation takes off from the heating surface, and, the fresh cooling water comes onto the heating surface to continue this boiling heat transfer process as depicted in Fig. 3a). Unless any bubbles swell on the heated surface, it could be cooled with higher heat flux under constant ΔT, as illustrated in Fig. 3b).

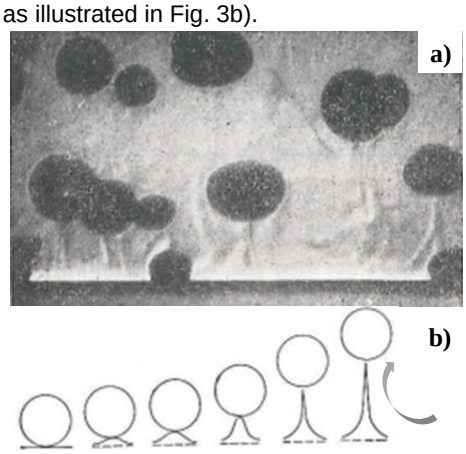

Figure 3. Take-off of growing vapor bubbles from the heating plate. a) Dynamic imagining, and b) a model of taking off process for vapor bubbles [6].

Authors discussed the effect of micro-/nano-texturing onto the aluminum and copper heating plate on the boiling heat transfer in the water – vapor system [13-15]. In parallel with those fundamental works, various micro-/nano-texturing methods have been developed by the previous studies; e.g., the plasma-oxidation assisted printing [16-18], the plasma-nitriding assisted printing [19-21] and the extremely short-pulse laser micro-/nano-texturing [22-24]. In the first approach, carbon-derivative coatings such as DLC (Diamond-Like Carbon), CNT (Carbon Nano-Tube) and diamond coatings were processed to yield those carbon-coated dies with microtextures [13-14, 25]. Those aspect ratio was predetermined by the coating thickness. In second, the selective nitrogen supersaturation process advanced into the unmasked surfaces and interfaces by the ink-jet printing [19-21], the screen printing [26-27] and the lithography [28-29]. In this case, the aspect ratio of micro-/nano-textures were determined by the nitrided layer thickness up to sub-mm thickness. In third, the nanotextured ripples superposed on the tailored micro-textured surface profile by the femtosecond laser processing [30]. In particular, the unidirectional nanotextures were simultaneously formed onto the trimmed tool surface [31-32]. On the basis of these micro-/nano-texturing methods, surface-topological design is performed to control the heat transfer process with phase transformation on the textured surface.

In the present paper, two microtexturing methods are employed to fabricate the textured aluminum and copper specimens for boiling heat transfer experiments. In the first method, the plasma-oxidation assisted micro-texturing is utilized to build up fine alignment of micro-square pillars on the thick DLC die. This convex microtextures are imprinted into the pure aluminum sheet for heat transfer experiment to describe the bubble nucleation and take-off behavior. At the presence of micro-cavities on the aluminum interface, the bubble size is reduced by 1/100 or less to be free from swelling on the interface by flowing away with the coolant. In the second method, the wet plating is utilized to form the acicular convex microtextures onto the oxygen-free pure copper specimen for heat transfer experiment to demonstrate the effect of coolant flow velocity on the boiling heat transfer. The heat flux increases to exceed CHF. Through these steps, a physical model is considered to design and fabricate the heat transfer device with $q > q_{cr}$ and $q >> q_{cr}$.

2. Experimental Procedures

2.1. Micro-texturing by plasma printing

The lithography with ion milling and reactive ion etching, as shown in Fig. 4a), was utilized to print the square unit cell pattern with the size of 3.5 μm x 3.5 μm and the pitch of 5 μm onto the DLC coated AISI420 punch with the coating thickness of 15 μm. After the procedure in Fig. 4b), the platinum deposit on the nano-carbon film was left as a unit cell.

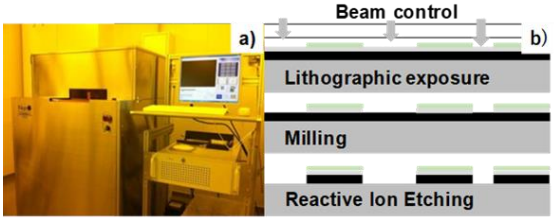

Figure 4. Lithographic micro-patterning onto thick DLC coated AISI420 die. a) Lithographic system, and b) illustration of micro-patterning process.

This die was subjected to etching by plasma oxidation to remove the unmasked DLC coating and to form the DLC micro-punch array on the DLC-coated AISI420 die.

2.2. Micro-texturing by wet plating

The wet plating was employed to form the acicular micro-pattern onto the oxygen-free copper specimen with use of nickel and iron ionized solution. The duration time in plating was varied to control the size and length of acicular Fe-Ni microtextures on the copper block.

2.3. Heat-transfer experimental setup

Two experimental set-ups were utilized to describe the vapour bubble nucleation and take-off and to demonstrate the effect of micro-textures on the boiling heat transfer process.

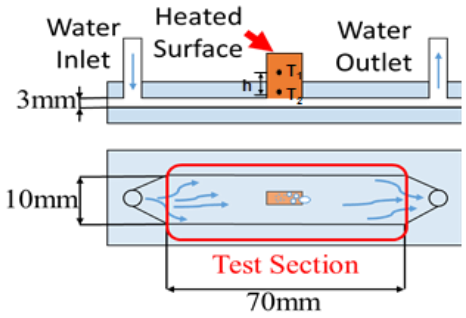

Figure 5. Direct observation of bubble nucleation and take-off in the boiling heat transfer on the micro-textured aluminum surface.

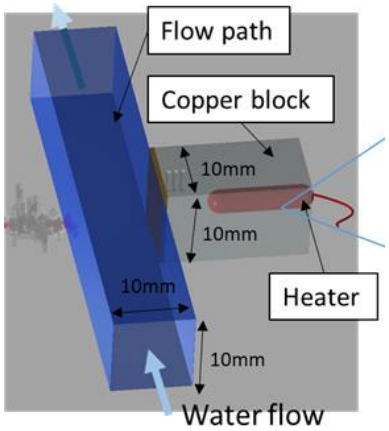

Figure 6. Boing heat transfer measurement on the micro-textured copper surface.

Figure 5 depicts a setup to describe the phase transformation behavior in the test section with the length of 70 mm under the uniform heating of flowing water by the copper block. Pure aluminum devices with and without microtextures were joined to the top of this block. The heat flux (q) through these devices was determined by the difference of temperature histories in the block. High speed video camera was utilized to visualize the vapor bubble nucleation and its take-off from the aluminum devices.

Figure 6 shows another setup to measure the heat transfer characteristics with the use of the heating copper block. The microtextures were directly formed onto this block. The water channel stood in vertical to control the flow velocity and to investigate the effect of forced cooling velocity on the heat transfer. The heat flux was measured in the similar manner to the setup in Figure 5.

3. Experimental Results

3.1. Fabrication of aluminium sheet with micro-cavities

Two dimensional micro-pattern was printed by the lithography onto the DLC film coated on the AISI420 substrate. A square dot with 3.5 μm x 3.5 μm is aligned with the pitch of 5 μm on this DLC coating as depicted in Fig. 7.

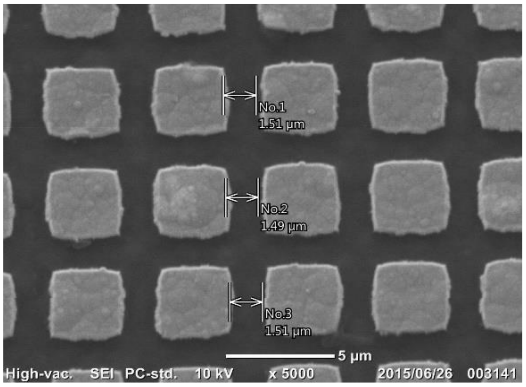

Figure 7. Micro-patterned DLC film coated on the SKD11 die by the lithography.

High density plasma oxidation process was utilized to chemically remove the unprinted DLC films. After plasma oxygen etching for 5 ks, DLC micro-pillared punch array was constructed by this selective removal of unprinted DLC films. Figure 8 depicts the SEM image of the arrayed DLC-punch with the square head by 3.5 μm x 3.5 μm and the height of 8 μm.

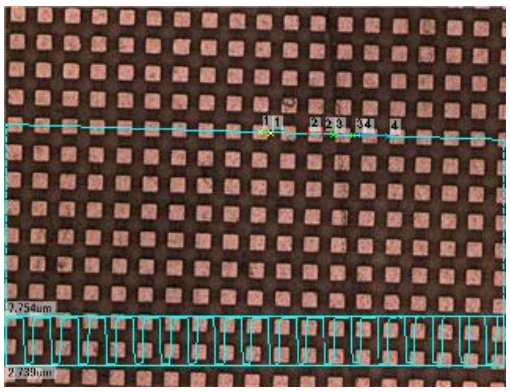

Figure 8. DLC arrayed punch with each head of 3.5 μm x 3.5 μm and height of 8 μm for precise imprinting into aluminium sheet.

The depth profile of DLC punch array was measured by the laser surface profilometer and supposed in Figure 8. DLC micro-punches with the head size are regularly aligned with the pitch of 5 μm by plasma oxidation etching of the micro-patterned DLC coating surface in Figure 7. This regular alignment of micro-punches proves the accurate imprinting of micro-textures into the metallic sheets and plates by the precise stamping with the use of this DLC-punch.

CNC (Computer Numerical Control) – stamper was

utilized for this imprinting of DLC punch array into the pure aluminium sheet with the thickness of 0.2 mm. Figure 9 depicts the aluminium sheet surface with the micro-cavity array, which is imprinted by indentation of the DLC-punch array in Figure 8.

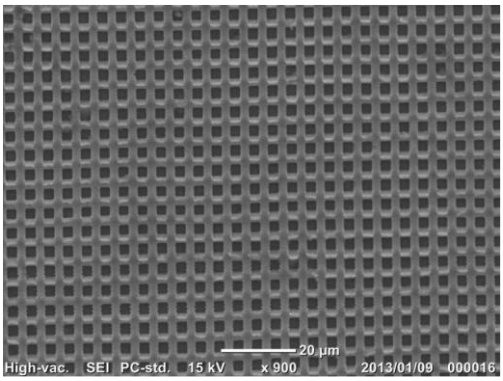

Figure 9. A pure aluminium sheet with the micro-cavity array formed by the indentation of the DLC-punch array in Figure 8.

In this indentation of DLC-punch array, the pure aluminium is backward extruded into the clearance between adjacent DLC-punches to form the thin walls with the thickness of 1.5 μm. Through this imprinting of each DLC-punch into aluminium sheet, its head shape of 3.5 μm x 3.5 μm makes a bottom of a micro-cavity. Four clearances surrounding each DLC-punch become four micro-cavity walls with the height of 5 μm.

This imprinting process incrementally advances by stamping the micro-textured AISI420 punch with the head size of 80 mm x 10 mm into the pure aluminium sheet. Each stamped aluminium sheet segment has 3.2×10^7 micro-cavities on its area of 80 mm x 10 mm. Then, the density of micro-cavities reaches to 4×10^4 /mm^2.

3.2. Bubble nucleation and growth

This pure aluminium segment with micro-cavity alignment was joined to the copper block by using the silver paste. Figure 10 compares the heating copper block before and after joining the aluminium segment.

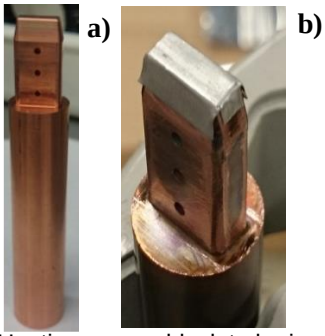

Figure 10. Heating copper block to be inserted into the experimental setup in Figure 5. a) The copper block without aluminum device, and b) the copper block with aluminum device.

In this setup, the phase transformation from the liquid water to vapor takes place on the surface of aluminium device with and without the micro-cavity textures. Figure 11a depicts the nucleation and growth of bubbles on the bare aluminum device without micro-textures. Large bubbles swell on its surface and grow by themselves.

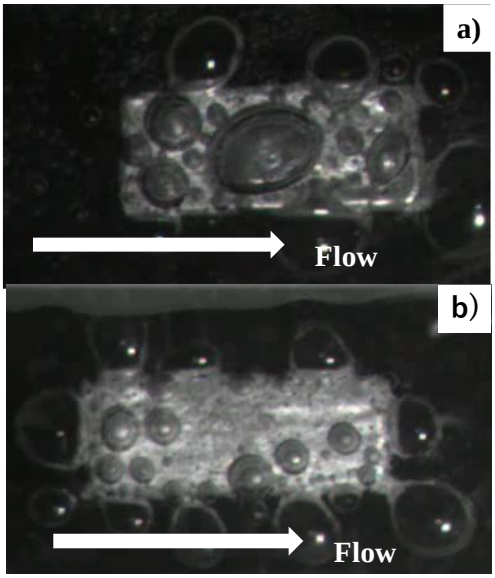

Figure 11. The bubble nucleation and growth on the aluminum device. a) without micro-cavity textures, and b) with micro-cavity textures.

As depicted in Figure 11b, only fine bubbles nucleate without significant growth. Most of them flow away together with coolant. This micro-texturing effect on the bubble nucleation and growth mechanism reflects on the heat transfer on the aluminum interface between the heating block and the coolant.

The heat flux was measured at each specified superheat ΔT with and without microtextures. Figure 12 compares this relationship between the measured heat flux and the superheat.

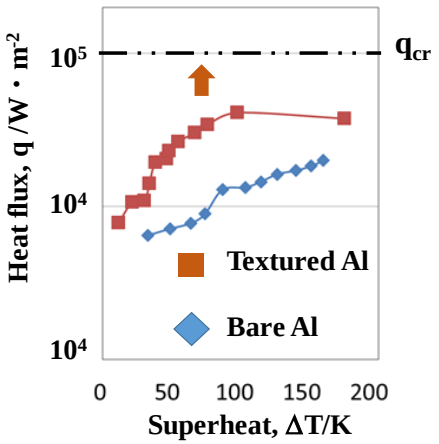

Figure 12. The relationship between q and ΔT on the aluminum device with and without the microtextures for the heat transfer experiment in Figure 4.

When using the bare aluminum device, the heat flux gradually increases with ΔT in correspondence to the normal heat transfer mechanism in Figure 1. On the other hand, at the presence of microtextures on the aluminum device, the heat flux steeply increases with ΔT at the beginning of superheating. Although this increasing heat flux is suppressed around ΔT = 60 K due to the insufficient coolant flow volume, the

microtextures enhance the increase of heat flux with ΔT so that q approaches to the critical heat flux, q_{cr}.

This heat transfer behavior through the micro-cavity arrayed aluminum device teaches:

1) the bubble size is reduced by decreasing the wedge size,
2) the onset superheat of ΔT_{onset} nearly goes toward zero, and
3) the heat flux q increases steeply toward the critical heat flux, q_{cr}.

After the classical theory, the effect of the wedge size on the heat transfer is considered by

$$\Delta T \sim 2\sigma T_{sat} / [\rho_v \cdot \Delta h_v \cdot r_c \cdot (1 - r_c/\delta)], \quad (1)$$

where σ is the thermal conductivity, T_{sat} is the saturated temperature, ρ_v is the mass density of coolant, Δh_v is the latent heat, r_c is the radius of wedge, and δ is the thermal boundary layer thickness. This theory predicts that the superheat increases with reduction of r_c. However, Figure 12 proves that ΔT_{onset} decreases with reduction of the micro-cavity size. This contradiction comes from the difference of fine bubbling mechanism on the interfaces without and with the regular micro-cavity alignment.

On the flat interface, each bubble is generated at the natural wedge by the phase transformation of coolant. Since every bubble is isolated from the neighboring bubbles, higher superheat is needed to enhance the nucleation and growth of bubble before its take-off from the wedge. On the other hand, lots of bubbles are generated at the regularly aligned wedges with the specified distance between adjacent wedges. In Figure 9, each wedge is distanced by 5 μm so that lower superheat is enough to generate a fine bubble under the surrounding coolant flows. As observed by the high speed camera in Figure 11, a mass of fine bubbles is easily moved with the coolant flow so that the interface returns to be back to the initial bubble-nucleation stage under the fresh coolant.

This first experiment with the use of regularly aligned wedge microtexture, demonstrates that the boiling heat transfer mechanism in Figure 1 is controllable by micro-texturing the interface between the coolant and the heating media and that higher heat flux is released by this micro-textured device.

Next, let us consider two engineering issues to advance this approach for controlling the boiling heat transfer by microtexturing.

One item is how to design the micro-textured interface properties in addition to the regular alignment of micro-cavities or wedges in Figure 9. Since the metal surface is usually hydrophilic with the static contact angle of 60° - 70°, this surface condition is controlled by micro-/nano-texturing to be more hydrophilic or to be hydrophobic, as an engineering policy. Another item is how to improve the q – ΔT relation-ship by the coolant design. Among several parameters, the coolant flow velocity is employed as an important item. After the classical treatise on the boiling heat transfer [6], its mechanism was considered to be invariant to the coolant flow velocity.

3.3. Fabrication of convex micro-textured specimen

The wet plating process was employed to build up the acicular iron – nickel alloy microtextures directly onto the copper heating block surface. Figure 13 depicts the heating copper block with the micro-textured Fe-Ni layer on its head surface.

Figure 13. A heating copper block with the micro-textured Fe-Ni layer on its head.

In the previous heating block in Figure 10, the micro-textured aluminium sheet was joined to the block. The measured q – ΔT relationship was biased by the thermal conductance of silver paste. In this setup, the micro-textured layer is directly deposited onto the heating block head surface. Hence, the geometric configuration of wet-plated Fe-Ni layer reflects on the surface property and on the bubble nucleation and growth during the boiling process.

Two Fe-Ni wet-plated layers with different micro-textures were prepared to investigate the role of their geometric configurations in the boiling transfer mechanism. Figure 14a depicts the microstructure of first Fe-Ni micro-textured specimen or specimen-1. The acicular unit cell with the bottom size of 0.2 – 0.5 μm and the height of 0.7 μm, aligns with the semi-regular spacing. As depicted in Figure 14b, this textured surface become hydrophilic with the contact angle of 20 – 30°.

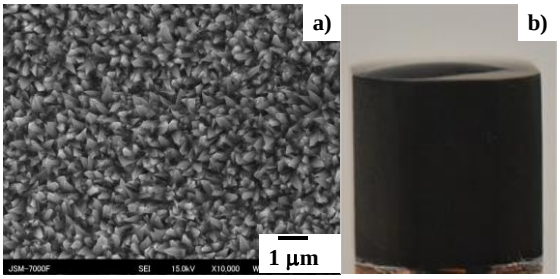

Figure 14. The first Fe-Ni micro-textured heating block specimen-1. a) Its microstructure in the plain view, and b) its wettability.

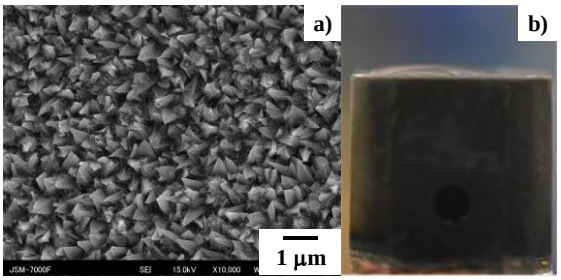

Figure 15. The second Fe-Ni micro-textured heating block specimen-2. a) Its microstructure in the plain view, and b) its wettability.

The second specimen or specimen-2 has nearly the same microstructure in Figure 15a as seen in Figure 14a. Its acicular unit cell has its bottom size of 0.2 – 0.7 μm and the height of 1 μm. After the wettability testing, this specimen is also hydrophilic with the same contact angle.

These two specimens are utilized for the boiling heat transfer experiments in Figure 6 to investigate the effect of the geometric topology on the q – ΔT relationship and the heat transfer mechanism.

3.4. Heat transfer on the micro-textured surface

Two types of experiments are performed; one for investigation on the effect of micro-texture topology on the heat transfer and the other for description on the effect of coolant velocity or Reynolds number (Re) to the heat transfer mechanism.

In the first experiment, the coolant velocity was preserved to be constant by V = 1.9 ml/s or Re = 460. In the similar manner, the coolant was degassed and its temperature was also controlled to be 347 K or subcooled by 30 K. The copper block was gradually heated by increasing the applied voltage in every 10 V.

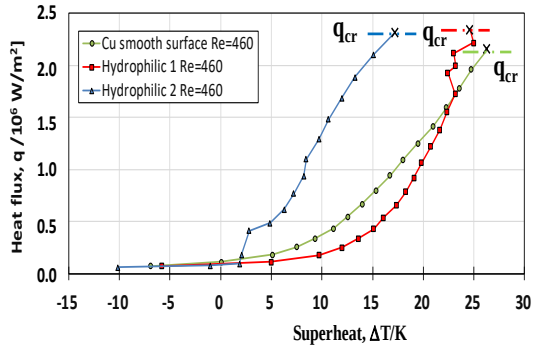

Figure 16. q - ΔT relationship for three specimens under Re = 460.

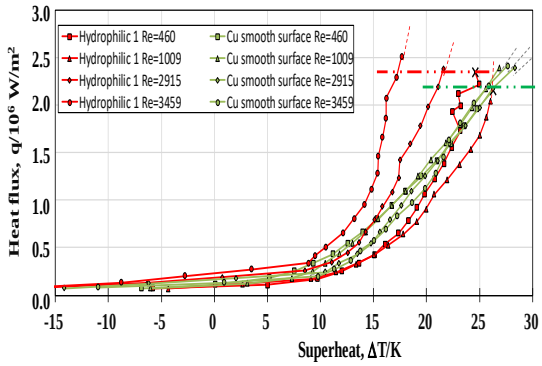

Figure 17. q - ΔT relationships for normal copper block without microtextures and specimen-1 with increasing Re.

As predicted from Figure 1, the heat flux increases gradually with increasing the superheat in case of cu-block without the microtextures. When using the specimen-2 with the microstructure in Figure 15, the heat flux abruptly onsets at ΔT = 2 K, rapidly increases with ΔT and approaches to the critical heat flux, q_{cr} at ΔT = 17 K. Since q = 0.5 x 10^6 W/m^2 at ΔT = 17K when using the copper block without the microtextures, five times higher heat flux is attained by using this hydrophilic microtexture.

On the other hand, in case of the specimen-1 in Figure 14, its q - ΔT relationship becomes nearly the same as q - ΔT for non-textured specimen. This implies that the boiling heat transfer behavior becomes sensitive to the acicular microtexture morphology under the laminated coolant flow.

In the second experiment, the coolant flow velocity was increased to change the laminated flow to the turbulent flow and to investigate the sensitivity of boiling heat transfer mechanism to the flow pattern change. Figure 17 compares the variation of q – ΔT curves with increasing the Re between the specimen-1 and the normal copper block without microtextures.

When using the bare copper heating block in Figure 6, four heat flux to super heat relationships become nearly the same even by increasing Re from 460 to 3459. This insensitivity of boiling heat transfer process to the coolant flow pattern change, just abides by the classical treatise [6]. As stated before, this insensitivity reveals that the bubble nucleation and growth process on the interface has nothing to do with the coolant flow behavior. This is because each wedge on the bare copper is isolated from each other and a bubble nucleates and grows mainly in the function of superheat.

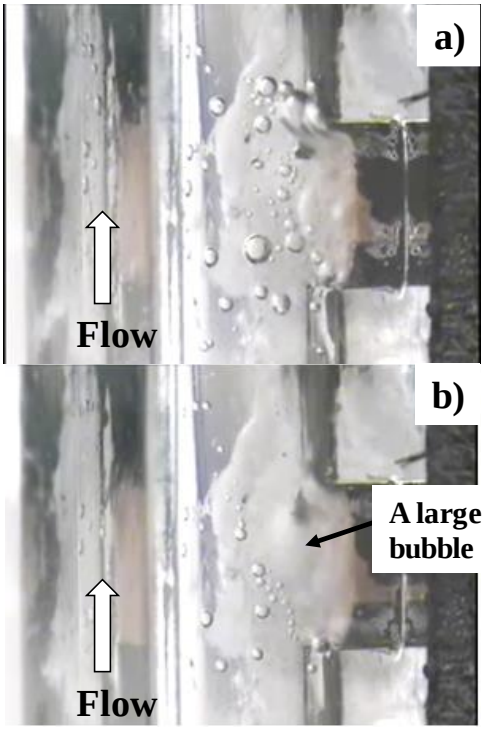

Figure 18. Snap shot of the boiling process above the bare copper block head without microtextures in the coolant channel at Re = 3459 with increasing the applied power (P) for heating. a) P = 110 W, and b) P = 180 W.

An overall boiling and flow behavior was observed during the heat transfer experiment. Figure 18 depicts the boiling and flow processes in the coolant channel under Re = 3459. When the electric power is applied to the heating unit by 110W, the coolant is boiled both in down- and upper- streams around the heating copper block head in Figure 18a. Although the small sized bubbles are seen in this boiled coolant, the boiled coolant region widens symmetrically in both

streams of coolant. There are no ways for fresh coolant to flow onto the heating copper block head.

As shown in Figure 18b, when increasing the power to 180 W, the boiled coolant regions are nearly the same as seen in Figure 18a. That is, the boiling behavior does not change even by increasing the applied power to the heating unit. To be noticed, larger bubbles are seen in Figure 18b. This proves that the generated bubbles are easy to agglomerate themselves and to form a larger bubble. If these large bubbles coalescence to a film at the vicinity of interface, the bubble boiling mode could change to the film boiling mode. The boiling behavior in Figure 18b continues to make a burn-out when the heat flux approaches to the critical one.

The difference of q – ΔT relationship in Figure 17 predicts that the variation of the boiling process in Figure 18 should be changed by the microtexturing on the heating copper block head.

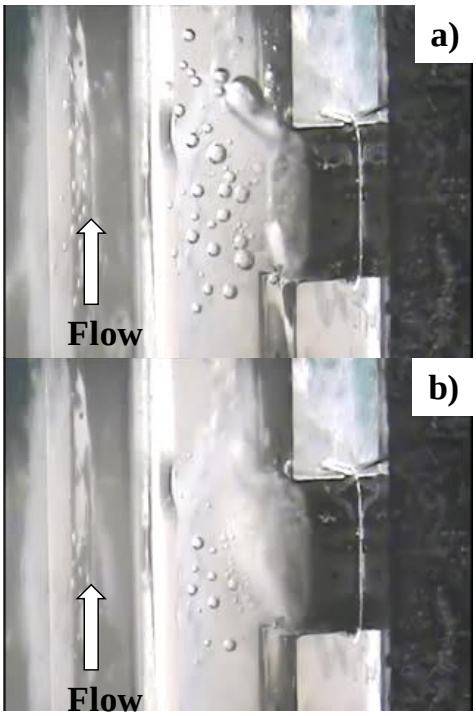

Figure 19. Figure 18. Snap shot of the boiling process on the micro-textured copper block head in the coolant channel at Re = 3459 with increasing the applied power (P) for heating. a) P = 110 W, and b) P = 180 W.

In the same experimental setup, the boiling behavior on the micro-textured copper block is monitored by high speed camera. When P = 110W, the boiling coolant region was seen only in the downstream and narrowed above the micro-textured interface between the heating copper block and coolant in Figure 19a. When increasing the applied power to 180 W, the bubbled coolant flows away in the downstream together with the coolant as seen in Figure 19b. To be noticed, a single-phase or liquid phase coolant comes from the upper-stream, mixes with the two-phase, turbulent flow from the interface, and flows away in the down-stream of channel in Figure 19.

This high speed camera observation on the flow pattern at Re = 3459 reveals that the coolant flow has significant interaction with the boiling heat transfer on the micro-textured interface. Two-phase mass with fine bubbles is moved away to the downstream of coolant. The micro-textured interface is cooled down by a new coolant from the upper-stream. These two steps work independently to sustain the higher heat transfer through the micro-textured interface. This results in the steep increase of heat flux to CHF and above CHF even at lower superheat.

3.5. Engineering toughness of microtextures in boiling

In the design of micro-textured devices, various engineering items must be taken into account. The regularly micro-textured aluminium sheets had mechanical strength and toughness against the severe attack of vapour bubbles and coolant pressure. However, the joined layer between aluminium sheet and heating block is a nuisance to influence on the measured heat flux by its thermal conductance.

The wet-plated acicular Fe-Ni microtextures are free from this disturbance to the heat transfer measurement. However, these are often damaged by erosion through the vapour bubble attack and coolant pressure.

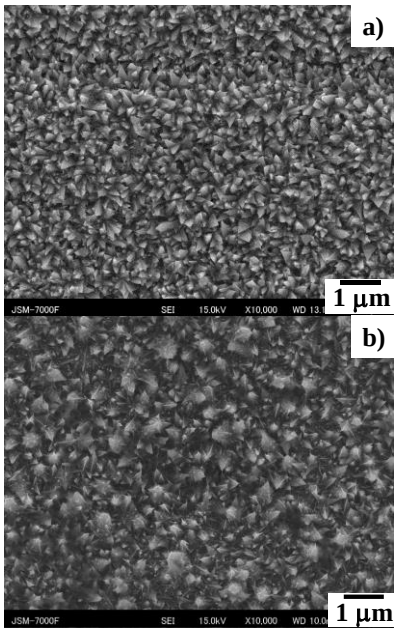

Figure 20. Comparison of microstructure for the wet-plated Fe-Ni microtexture with the bottom size of 0.1 to 0.4 μm and the height of 0.5 μm before and after the boiling heat transfer experiment.

Figure 20 compares the microstructure of the wet-plated Fe-Ni microtextures before and after the boiling heat transfer experiments. The initial microtexture has regular alignment of acicular pillars. Those were diminished severely enough to defocus the SEM observation in Figure 20b. That is, the wet-plated Fe-Ni deposits on the copper block head is easy to be eroded by the attack of bubbles under the coolant pressure.

4. Discussion

The micro-/nano-texturing onto the heating device surface has a significant influence on the boiling heat transfer. First, the heat flux to superheat relationship

in Figure 1 is controlled by the micro-/nano-texturing to have:

(1-1) the super heat to onset the boiling heat transfer is much reduced to nearly $\Delta T_{onset} \sim 0K$,

(1-2) the increase of heat flux by ΔT becomes steep along B - C - D curve, and

(1-3) the heat flux can exceed the critical heat flux (CHF).

In second, the classical model on the nucleation and growth of vapor bubbles in Figure 2 is exchanged with a new physical model, where:

(2-1) each bubble is nucleated in the designated alignment by the micro-/nano-texturing, and

(2-2) onset of phase transformation from the liquid coolant to the vapor is dependent on the local geometric topology of micro-/nano-textures.

In third, the classical measurement on the take-off of bubbles in Figure 3 is also exchanged with a new mechanical model where:

(3-1) the nucleated vapor bubbles are unstable on the micro-/nano-textured heating surface enough to take off at the early stage of superheating, and

(3-2) local mass in two-phase with lots of fine Bubbles, moves away with main turbulent flow of coolant.

Standing on these engineering items, let us describe the boiling heat transfer process through the micro-/nano-textured heating surface.

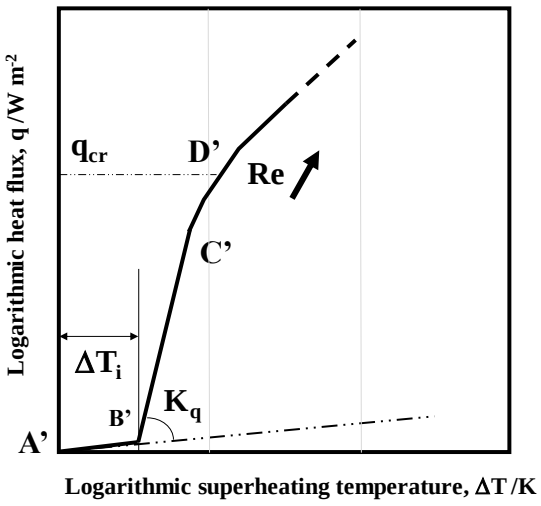

Figure 21. A physical model of the boiling heat transfer process on the micro-/nano-textured heating surface.

Figure 21 summarizes the heat flux to superheat relationship by the present physical model on the boiling heat transfer through the micro-/nano-textured heating surface. The boiling process starts at B' or at $\Delta T = \Delta T_i$. This intrinsic superheat (ΔT_i) is determined by the minimum thermal conductance of the micro-/nano-textured layer. Along the line B' to C', the heat flux increases with the steep gradient of K_q under the laminated coolant flow. This K_q is strongly dependent on the geometric topology of micro-/nanotextured layer. At C', the heat transfer process is enhanced by the coolant flow pattern change from the laminated flow to the forced turbulent flow. Under the continuous mass transfer of two-phase coolant with dense fine bubbles to the main flow, the heat flux exceeds the CHF and increases monotonously with ΔT above CHF.

Figures 12 and 16 reveal that this ΔT_i is less than 10 K and that K_q reaches to 0.2 x 10^6 W/($m^2 \cdot K$). Significant reduction of ΔT_{onset} to ΔT_i in these Figures teaches that phase transformation does not start at the single selected wedge but commences at every spot near the aligned micro-textures at the same time. Micro-/nano-texturing onto the heating surface stimulates the onset of bubble nucleation in the network of micro-cavities in Figure 12 and in the micro-pillars in Figure 16. That is, the mode change from the convection heat transfer process to the boiling heat transfer process, is triggered by the simultaneous nucleation of fine bubbles in mass.

The least superheat of ΔT_i is needed for thermal conductance of micro-/nano-textured layer. The difference of ($\Delta T_{onset} - \Delta T_i$) is wasted to homogenize each local bubbling process when using the heating surface without the micro-/nano-textures. This difference approaches to zero, or, $\Delta T_{onset} = \Delta T_i$ under simultaneous nucleation of fine vapor bubbles due to the micro-/nano-texturing.

The steep branch at B' with high gradient of K_q implies that the nucleated fine bubbles are easy to take off from the heating surface to the main stream of coolant. Once the nucleation mode changes to the growth mode of bubbles, the increase of heat flux by ΔT becomes redundant and slow. In particular, $q/\Delta T$ in the forced turbulent coolant flow regime, is still large enough to sustain the flow interaction between the generated two-phase local flow and the main forced coolant flow.

The effect of microtextures on the wettability has been discussed in the literature [30]. In case of heat transfer, high surface energy surface is preferable to cover the whole surface by coolant liquid and easy to release the nucleated bubbles. This suggests that the micro- and nano-textures must be designed with consideration on the multiple functions in the boiling heat transfer mechanism.

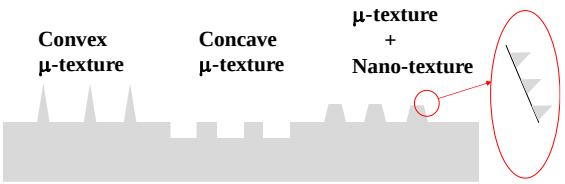

Figure 22. Topological design of the micro-/nano-textured surface with multiple role in the boiling heat transfer mechanism.

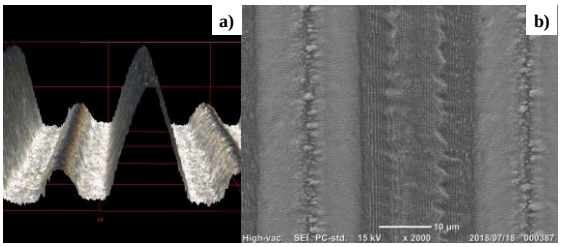

Figure 23. A micro-/nano-textured surface with the fractal dimension of 2.223 to be hydrophobic by the static contact angle of 170°. a) Surface profile of micro-/nano-textures, and b) its top view by SEM.

As illustrated in Figure 22, various microstructures are available to modify the heating surface conditions. In addition, various nanotextures are also formed onto each specified microstructure surface. Let us consider how to design the micro-/nano-textures to improve the coefficient of K_q at B' in Figure 21. There are two design items; e.g., a hydrophilic or super-hydrophilic surface texture design, and, a hydrophobic or super-hydrophobic surface texture design. The former was proved to be useful to control the boiling heat transfer in the present study. As seen in the difference between the specimen-1 and -2 in Figure 16, inhomogeneity in the surface condition becomes an issue of nuisance in practice.

As had been discussed in [22-24], the heating surface can be modified to be super-hydrophobic with the static contact angle of 170°. Figure 23 shows a typical micro-/nano-textured surface by the laser micromachining. Through this surface modification, the original two-dimensional surface turns to have much higher fractal dimension than 2.0. In addition to this self-similar surface condition, each microtexture surface is nanotextured with different orientation and period from each other. This microscopic peak to valley ratio has influence on the boiling heat transfer mechanism. The micro-bubbles are generated at the nanotexture edge and corner, and, they flow away with fresh coolant at the microtexture surface. The boiling process on the self-similar heating surface must be significantly different from the conventional physical model in Figures 1 to 3.

In addition to the scientific understanding on the effect of micro-/nano-textures to the boiling heat transfer, how to make mass production of the textured heat-transfer devices must be also taken into account. In the present paper, a mother DLC-coating die is built up to have tailored micro-/nano-textures by the plasma oxidation-assisted printing in order that these are imprinted onto the product surfaces. As demonstrated in [33-36], the nitrogen supersaturated stainless steel dies as well as the thick DLC coating punch are micro-/nano-textured by the laser micromachining as a mother tool. The LIPSS (Laser-Induced Periodical Surface Structured)-nanotextures are precisely imprinted to metal plates and sheets by CNC-stamper. Through this precise stamping, the mother topology of micro-/nano-structures as well as the tailored function are imprinted onto the product surfaces.

The other method is a coating procedure including the dry- and wet-plating to form the micro-/nano-textures directly onto the product surfaces. As shown in the acicular pillar formation in Figures 14 and 15, the anisotropic deposition or etching plays a key technique to form the convex and concave microtextures. As stated before, these textured layer must be post-treated to have high hardness and strength against the erosion by the vapor bubble attack. Once these micro-/nano-texture layers are hardened and strengthened, the product surfaces can be functionally decorated by the tailored coating with complex topology.

5. Conclusions

The boiling heat transfer process is significantly controlled by micro- and micro-/nano-texturing on the interface between the flowing coolant and the heated solid. The nucleation process of ultra-fine bubbles is put into practice when using the pure aluminum sheet and plate with regular alignment of micro-cavities on the heating block. Since these nucleated bubbles flow away with coolant without swelling onto the interface, its surface is covered by fresh coolant to sustain the high heat flux through the micro-textured interface.

The heat flux to superheat relationship is much improved by the micro-/nano-texturing. The heat flux starts to steeply increase by itself even at the lower super heat. This increase is enhanced with increasing the coolant velocity. Under the forced turbulent coolant flow, the mass of two-phase local flow with fine bubbles takes off from the textured surface and moves away to the down-stream of coolant. Since the fresh coolant flows onto the textured surface, the higher heat flux is sustained on the textured heating interface.

The present study starts to consider how to tailor the micro-/nano-textures for each boiling heat transfer design. Much more scientific idea and engineering effort is still necessary to find a way to release the much higher heat flux from the heating device and product surfaces to the coolant flow and to establish the thermal cycle with high efficiency.

Acknowledgements

The authors would like to express their gratitude to Dr. T. Yamada, Mr. M. Tasaka, Mr. S. Suwa (Graduate School of Science and Engineering, SIT) and Mr. H. Nakata (Ebina Chemicals, Co., Ltd.) for their help in experiments.

References

[1] D.B. Tickerman, R.F.W. Pease, High-performance heat sinking for VLSI. IEEE Electron Device Letters. 1981, EDL-2 (5), 126-129.

[2] L. Gong, J. Zhao, S. Huang, Numerical study on layout of micro-channel heat sink for thermal management of electric devices. Appl. Thermal Eng., 2015, 88, 480-490.

[3] S. Huang, J. Zhao, L. Gong, X. Duan, Thermal performance and structure optimization for allotted microchannel heat sing. Appl. Thermal Eng., 2017, 115, 1266-1276.

[4] P. Li, Y. Luo, D. Zhang, Y. Xie, Flow and heat transfer characteristics and optimization study on the water-cooled microchannel heat sinks with dimple and pin-fin. Int. J. Heat Mass Transfer, 2018, 119, 152-162.

[5] J.Y. Chang, S.M. You, Enhanced boiling heat transfer from micro-porous surfaces: effects of a coating composition and method. Int. J. Heat Mass Transfer. 1997, 40 (18), 4449-4460

[6] Y. Kattoh, Fundamentals in Heat Transfer. Yokendo: 1964.

[7] C. Sodtke, P. Stephan, Spray cooling on micro structured surfaces. Int. J. Heat Mass Transfer. 2007, 50, 4089-4097.

[8] T.J. Hendricks, S. Krishnan, C. Choi, C-H. Chang, B. Paul, Enhancement of pool-boiling heat transfer using nanostructure surface on aluminum and copper. Int. J. Heat Mass transfer. 2010, 53, 3357-3365.

[9] H. S. Ahn, C. Lee, H. Kim, H. Jo, S-H. Kang, J. Kim, J. Shi, M.H. Kim, pool boiling CHF enhancement by micro/nanoscale modification of zircaloy-4 surface. Nuclear Eng. Design, 2010, 240, 3350-3360.

[10] H. Jo, H. S. Ahn, S-H. Kang, M.H. Kim, A

study of nucleate boiling heat transfer on hydrophilic, hydrophobic and heterogeneous wetting surfaces. Int. H. Heat Mass Transfer. 2011, 54, 564305652.
[11] S.M. Jung. D.J. Preston, H.Y. Jung, Z. Deng, E.N. Wang, J. Kong., Porous Cu nanowire aerosponges from one-step assembly and their applications in heat dissipation. Adv. Mater. 2016, 28, 1413-1419.
[12] G.J. Simitses, D.H. Hodges, Fundamentals of structural stability. Butterworth Heinemann, 2006.
[13] T. Aizawa, M. Tamaki, T. Fukuda, Large area micro-texture imprinting onto metallic sheet via CNC stamping. J. Procedia Eng. 2014, 81, 1427–1432.
[14] T. Aizawa, T. Fukuda, Pulsewise-motion controlled stamping for micro-texturing onto aluminum sheet. J. Micro-Nano Manuf. ASME 2016, 4, 014502 - 014511.
[15] T. Aizawa, K. Wasa, H. Tamagaki, A DLC-punch array to fabricate the micro-textured aluminum sheet for boiling heat transfer control. micromechanics. MDPI 2018, 9, 147, 1-10.
[16] T. Aizawa, T. Fukuda, Oxygen Plasma Etching of diamond-like carbon coated mold-die for micro-texturing, Surf. Coat. Technol. 2013, 215, 364-368.
[17] T. Aizawa, Micro-texturing onto amorphous carbon materials as a mold-die for micro-forming. Applied Mechanics and Materials 2014, 289, 23-37.
[18] T. Aizawa, Micro-texturing for tribology and surface engineering in manufacturing process, Proc. 4th ISAST Conference, Indonesia 2016, 1-17.
[19] T. Aizawa, H. Suga. T. Yamaguchi: Plasma-nitriding assisted micro-texturing into stainless steel molds. Proc. 4th ICNFT 2015, 9002/1 – 9002/6.
[20] T. Aizawa, T. Takashima, T. Shiratori: Plasma printing to fabricate the micro-piercing dies for miniature metal products. Proc. 8th AWMFT 2015, J1/1 – J1/6.
[21] T. Nagata, T. Aizawa: Plasma-nitriding assisted modification of stainless steels for micro surgery knives. Proc. 11th ICOMM 2016, 59, 1-5.
[22] T. Aizawa, T. Inohara, Pico- and femtosecond laser micromachining for surface texturing. Micromachining, Ch. 7 Intech Open 2019, 1-24.
[23] T. Hasegawa, T., Aizawa, T. Inohara, S-I. Yoshihara, Mold-stamping of optical glasses by micro/nano-textured die to transcript the hydrophobicity. J. JSTP 2019, 60, 23-27.
[24] T. Aizawa, T. Inohara, K. Wasa, Femtosecond laser micro/nano-texturing of stainless steels for surface property control. micromachines, 2019, 10, 512, 1-10.
[25] E.E. Yunata, T. Aizawa: Micro-grooving into thick CVD diamond films via hollow cathode. Manufacturing Letters. 2016, 4, 17-22.
[26] T. Shiratori, T. Aizawa, Y. Saito, K. Wasa, Plasma printing of an AISI316 micro-meshing punch array for micro-embossing onto copper plates. J. Metals 2019, 9, 396, 1-11.
[27] T. Aizawa, Y. Saito, H. Hasegawa, K. Wasa. Fabrication of optimally micro-textured copper substrates by plasma printing for plastic mold packaging. Int. J. Automation Technology 2020, 14, 2, 200-207.
[28] T. Aizawa, Development of micro-manufacturing by controlled plasma technologies. J. Jpn. Soc. Technol. Plast. 2017, 58, 1064–1068.
[29] T. Aizawa, S-I. Yoshihara, Microtexturing into AISI420 dies for fine piercing of micropatterns into metallic sheets. J. JSTP 2019, 60, 53–57.
[30] T. Aizawa, T. Inohara, K. Wasa, Fabrication of super-hydrophobic stainless steel nozzles by femtosecond laser micro-/nano-texturing. Int. J. Automation Engineering 2020, 14,2, 159-165.
[31] T. Aizawa, T. Shiratori, T. Yoshino, T. Inohara, Femtosecond laser trimming of CVD-diamond coated punch for fine embossing. Mater. Trans. 2020, 61, 2, 244-250.
[32] T. Aizawa, T. Shiratori, Y. Kira, T. Inohara, Simultaneous nano-texturing onto CVD-diamond coated piercing punch with femtosecond laser trimming. J. Appl. Sci. 2020, 10, 2674, 1-13.
[33] T. Aizawa, T. Yoshino, T. Inohara, Micro-/nano-texturing of aluminum by precise coining for functional surface decoration. J. Metals 2020, 10, 1044, 1-10.
[34] T. Aizawa, T. Inohara, K. Wasa, Nano-texturing onto tool-surface by the femtosecond laser processing. Proc. WCMNM-2021 (September, 2021; India, Mumbai) (in press).
[35] T. Aizawa, T. Yoshino, T. Shiratori, T. Inohara, Femtosecond laser printing of micro-/nano-textures into DLC dies for functional decoration of light metals. J. Nanomaterial 2021 (in press).
[36] T. Aizawa, T. Yoshino, Y. Suzuki, T. Komatsu, T. Inohara, Micro-/nano-texture surface decoration of metals and metallic alloys via femtosecond laser processing and precise imprinting. Proc. 13th AFGS (December, 2021; China, Hong Kong) (in press).